Supporting Information

Control of Excited-State Proton-Coupled Electron Transfer by Ultrafast Pump-Push-Probe Spectroscopy in Heptazine-Phenol Complexes: Implications for Photochemical Water Oxidation

Kathryn L. Corp[†], Emily J. Rabe[†], Xiang Huang[╬], Johannes Ehrmaier[╬], Mitchell E. Kaiser[†], Andrzej L. Sobolewski[§], Wolfgang Domcke[╬], and Cody W. Schlenker[†⊥┣*]

[†]Department of Chemistry, University of Washington, Seattle, Washington 98195, United States
[⊥]Molecular Engineering & Sciences Institute, University of Washington, Seattle, Washington 98195, United States
[┣]Clean Energy Institute, University of Washington, Seattle, Washington 98195, United States
[╬]Department of Chemistry, Technical University of Munich, D-85747 Garching, Germany
[§]Institute of Physics, Polish Academy of Sciences, PL-02-668 Warsaw, Poland

Table of Contents

SECTION I: MATERIALS AND METHODS

Reagents.

Urea, potassium hydroxide, phosphorous oxychloride, phosphorous pentachloride, and phenol were purchased from Sigma Aldrich. Anisole (99%), 4-chlorophenol, 4-methylphenol (p-cresol), and 4-methoxyphenol were purchased from Alfa Aesar. Aluminum chloride was purchased from Fischer Scientific. Toluene was purchased from various suppliers and distilled under argon atmosphere. All reagents were used without further purification.

Synthesis.

Graphitic carbon nitride: Briefly, urea (10 g) was heated in a porcelain crucible (20 mL) using a potter's kiln at 500 °C for 3 h, with a ramp rate of 30 °C per hour under ambient atmosphere. The light-yellow product was ground thoroughly with a mortar and pestle prior to use in further reactions.

Potassium cyamelurate: 4.5 g of graphitic carbon nitride was refluxed in KOH (3.0 M, 150 mL) for 6 h. The solution was hot filtered over a glass frit and then cooled for recrystallization. The resulting white crystals were filtered and washed with cold ethanol.

Cyameluric chloride: Phosphorous oxychloride ($POCl_3$) (35 mL) was added to a flame-dried round-bottom flask with a stir bar. Phosphorous pentachloride (4.6 g) was added and allowed to stir for 5 minutes. Potassium cyamelurate (2.0 g) was added and the suspension was refluxed under N_2 at 110°C for 6 hrs. $POCl_3$ was removed under reduced pressure using a distillation set-up in the fume hood. The remaining solution was put on ice and ice water (50 mL) was added dropwise while stirring. The product was vacuum filtered and washed with ice-cold water. The resulting product was dried under vacuum for a few hours and stored in a desiccator. Safety note: $POCl_3$ and PCl_5 react with water exothermically to produce HCl gas and H_3PO_4. Always keep these reagents in a ventilated chemical fume hood and quench slowly with sodium bicarbonate.

2,5,8-tris(4-methoxyphenyl)-1,3,4,6,7,9,9b-heptaazaphenalene (TAHz): Anisole (10 mL) was purged with nitrogen. Aluminum chloride (4.0 g) was added to the flask and allowed to stir for a few minutes at 60°C. Cyameluric chloride (1.0 g) was added slowly over 30 minutes. The reaction mixture was stirred at 60°C under nitrogen for 5 hours. Deionized water (25 mL) was added and the solution was stirred until the color changed to yellow and the large chunks dissolved. The resulting bright yellow powder was filtered and washed with water. The product was purified by slowly recrystallizing in hot DMSO (3 mg/mL). Characterization of TAHz is shown in our previous manuscript.[1]

Time-Resolved Photoluminescence Spectra.

Time-resolved photoluminescence spectra were collected using a Hamamatsu streak camera (C10910) with a slow-sweep unit (M10913-01) in photon counting mode. Samples were irradiated with 50 fs pulses at 365 nm and 1 kHz pump from a Coherent/Light Conversion OPerA solo optical parametric amplifier (OPA). Pump fluences were ~1 x 10^{13} photons/cm^3.

Laser Beam Characterization.

The pump beam profile was characterized at the sample position using the BC106N-VIS CCD Camera Beam Profiler purchased from Thorlabs. Spatial beam images and spot size calculations were obtained from Thorlabs' standard beam profiler software package. Average power was measured using the Coherent FieldMate laser power meter equipped with the OP-2 VIS high sensitivity sensor purchased from Edmond Optics.

Transient Absorption Spectroscopy.

Samples were irradiated with the 365 nm (~3 x 10^{14} photons/cm^3/pulse) output of a Coherent, Inc./Light Conversion OPerA Solo OPA that was pumped with 50 fs pulses from a 1 kHz Ti:sapphire amplifier (Libra-HE, Coherent, Inc.). Supercontinuum probe pulses (~200 fs) were generated by focusing a fraction of the 800 nm amplifier output onto CaF_2 or sapphire plates. The probe beam was temporally delayed from the pump using a mechanical delay line (Ultrafast Systems). Spectra were collected with a CMOS sensor and InGaAs fiber-coupled multichannel photodiode array spectrometer and plotted as the differential optical density, $\Delta OD(\lambda, t) = Pump_{on}(\lambda,t) - Pump_{off}(\lambda,t)$. A reference line was monitored to account for fluctuations in the probe beam. Spectra were measured in a 2 mm path length quartz cuvette with continuous stirring.

Global analysis.

To deconvolute time-resolved spectra, global analysis was performed using Glotaran, a graphical user interface for the R-package TIMP.[2] The analysis performed here contained two spectral components, according to the singular value decomposition, each with their respective decay constants. No parameters were constrained.

Pump-Push-Probe Spectroscopy.

Samples were pumped with the 365 nm (500 Hz) output of a Coherent, Inc./Light Conversion OPerA Solo OPA, and then pushed with the 1150 nm (1000 Hz) output of a Coherent, Inc./Light Conversion Topas OPA. The delay of the push was fixed 6 ps after the pump pulse. At various delays after the pump, the sample was probed (1000 Hz) with a white light continuum and the difference signal was collected and plotted as the differential optical density, $\Delta OD(\lambda, t) = Pump_{on}Push_{on}(\lambda,t) - Pump_{off}Push_{on}(\lambda,t)$.

Electron Paramagnetic Resonance (EPR) Spectroscopy.

Samples were prepared in an argon glovebox in flame dried glassware. Air-free toluene from a still was added to each vial to prepare stock solutions of TAHz, 5,5-dimethyl-1-pyrroline N-oxide (DMPO, a common radical-scavenging spin-trapping agent, *cf.* Figure S1), and each respective R-PhOH species. Sample solutions (100 uM TAHz, 50 mM DMPO and 45 mM R-PhOH) for representative spectra in Figures S1a and S1b were prepared from the stock solutions just prior to the measurements and transferred to an air-free EPR tube. Samples for the lifetime measurements (100 uM TAHz, 150 mM DMPO and 135 mM R-PhOH) were illuminated and measured over time until the signal intensity dropped to zero. The same aliquot was then illuminated again and measured for a total of 4 cycles. Electron paramagnetic resonance (EPR) spectra were collected on a Bruker EMXnano X-band spectrometer with a 100 kHz magnetic field modulation and a 9.64 GHz microwave source equipped with Bruker Xenon software for data acquisition. The field was centered at 3442 gauss with a 100 gauss sweep, 20 dB attenuation, and a modulation intensity of 2 gauss. The sweep time was 2 seconds with a 100 ms delay in between each acquisition. Samples were excited under 365 nm illumination from an array of Marktech Optoelectronics LEDs (MTSM365UV4-F30115S) for 5 min prior to data acquisition.

The representative spectra shown in Figure S1 of spin-trapped radical products of photoreactions of TAHz with either PhOH or MeO-PhOH are an average of 15 acquisitions. In order to account for possible variations

in the lifetime of the phenoxyl radical adducts, samples were illuminated and 160 sequential acquisitions were obtained over time. A polynomial baseline fit was subtracted from each acquisition in order to shift the baseline to zero. The result was numerically integrated twice to obtain the area under the absorbance spectra, which is directly proportional to the number of spins in the sample. The intensity was then plotted against time and a monoexponential fit was used to determine the lifetime of the radical species as the inverse of the exponential rate. Because the samples of the different phenols were measured in identical tubes with the same volume, the instrument settings were constant between samples, the Q-factor was the same and the radicals measured are both oxygen-centered on the same spin trap, this intensity can be used to compare relative number of spins between samples.

SECTION II: ADDITIONAL SPECTROSCOPIC DATA

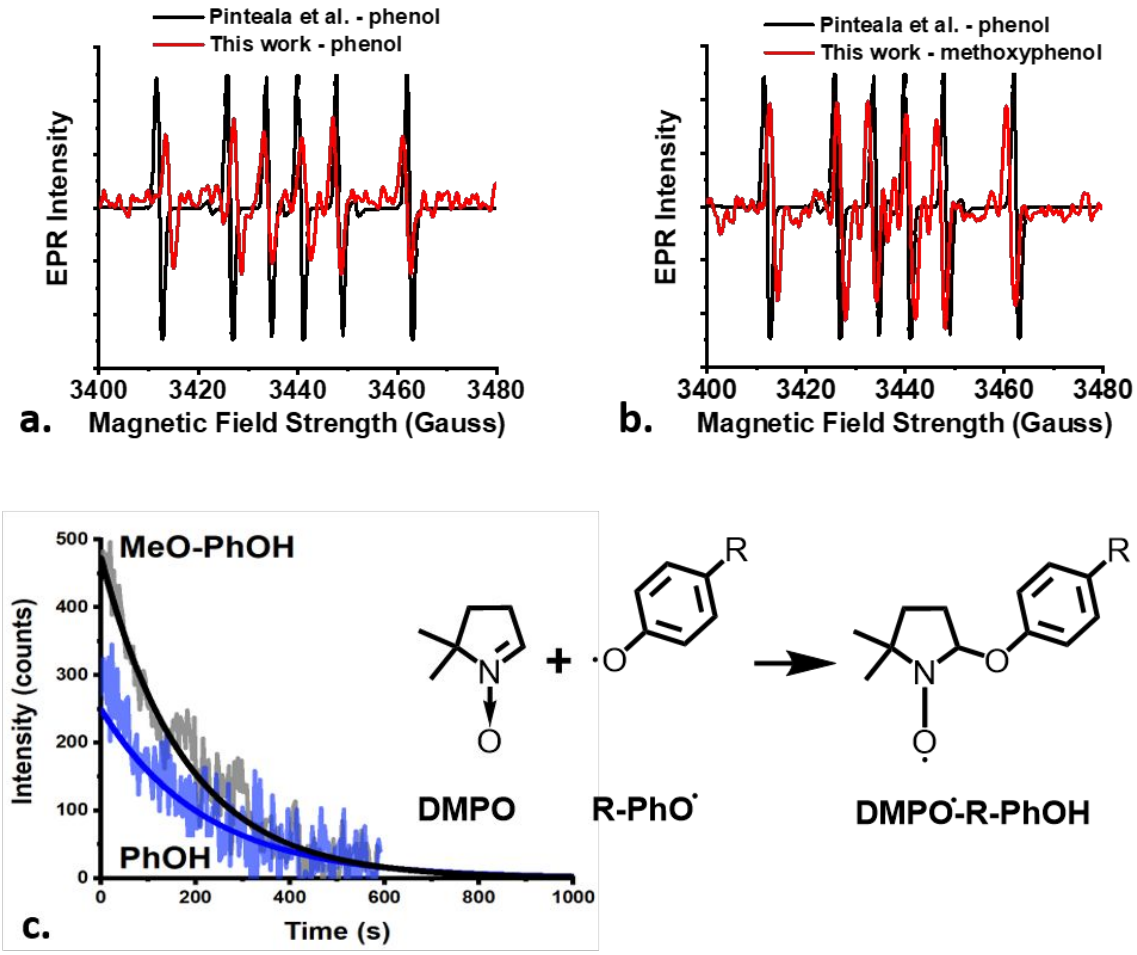

Figure S1. a) Spin-trapping EPR signal from phenoxyl radical/DMPO adduct following excitation of a TAHz solution in air-free toluene with 365 nm light (red trace) overlaid with a literature spectrum from Pinteala et al.[3] or the phenoxyl radical/DMPO adduct (black trace). b) Spectrum for analogous experiment to that presented in Figure S1a but with MeO-PhOH substituted for PhOH shown in red. The black trace is a reproduction of the literature phenoxyl adduct spectrum in part a) for reference. c) Numerically integrated EPR signals proportional to spin concentration for PhOH and MeO-PhOH spectra shown in a) and b), respectively. The initial signal amplitude for the MeO-PhOH sample is roughly 40% greater than that of the PhOH sample, indicating a larger R-phenoxyl radical yield for TAHz:MeO-PhOH, despite the spin-trapped DMPO-MeO-PhO radical adduct exhibiting a shorter lifetime. Inset: DMPO spin-trapping reaction.

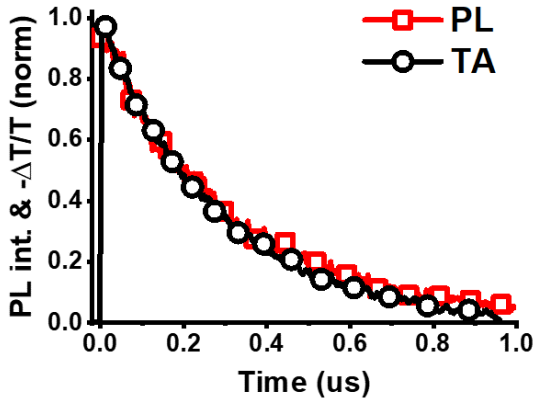

Figure S2. Photoluminescence (480 – 520 nm) and transient absorption (900 – 1000 nm) decays of TAHz (30 μM) in toluene. Both traces are normalized to the maximum population at time zero. This demonstrates that the induced absorption and the photoluminescence are likely arising from the same excited-state species.

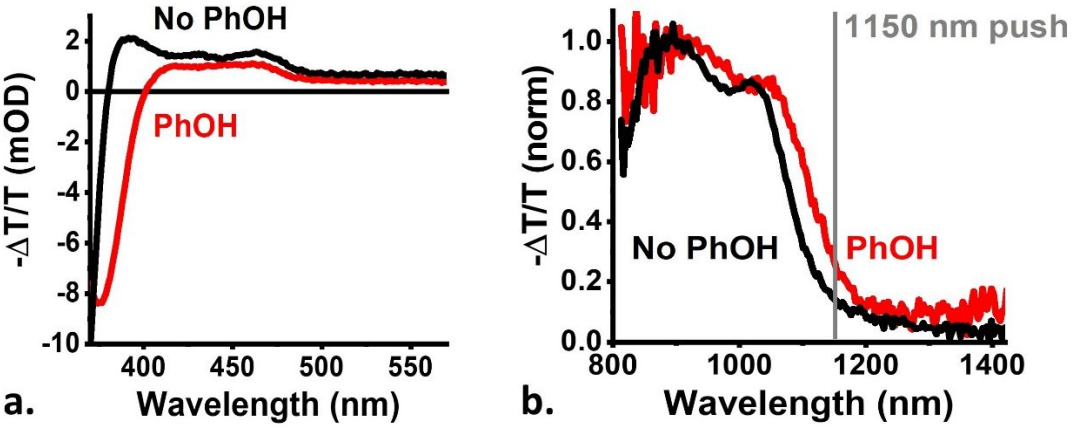

Figure S3. Transient absorption spectra of TAHz (50 μM) in toluene with (red) and without (black) phenol, PhOH (1.0 M). Spectra were averaged from 2-3 ps in (a) the ultraviolet/visible and (b) in the near-infrared where they were normalized at 900 nm. This demonstrates a slight red shift due to the hydrogen bonding environment when PhOH is present.

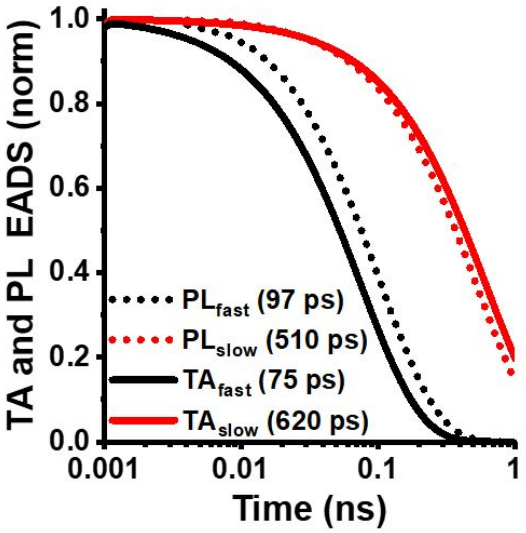

Figure S4. The normalized transient absorption (TA) and photoluminescence (PL) evolution associated decays (EADS) show two components with nearly identical decays. This suggests luminescent species are the species being probed by transient absorption (pump-probe) spectroscopy. Data was collected with 15 μM TAHz in toluene with 1.0 M PhOH.

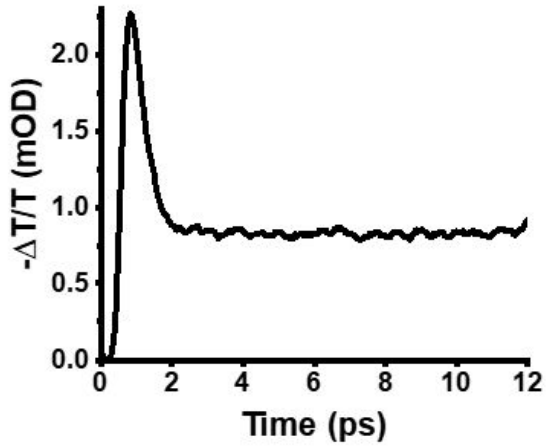

Figure S5. The decay of the excited-state population of TAHz monitored from 500-550 nm in the presence of PhOH (1.0 M) in toluene demonstrating the sub-picosecond relaxation of the S_n state after 365 nm excitation. Solvent reorganization is likely included in this relaxation.

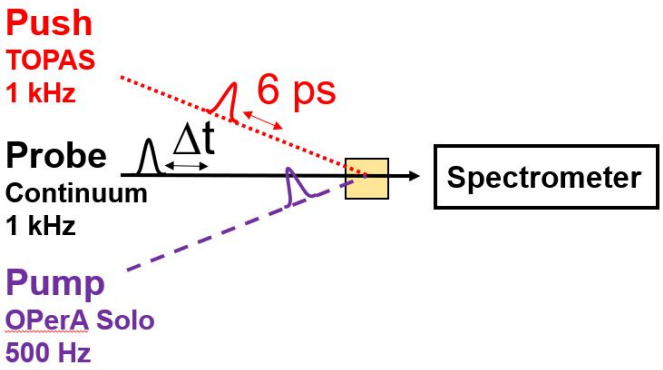

Figure S6. Diagram of pump-push-probe beam overlap and timing. The push in this work is fixed at roughly 6 ps. The probe in this manuscript was delayed from 0 – 12 ps.

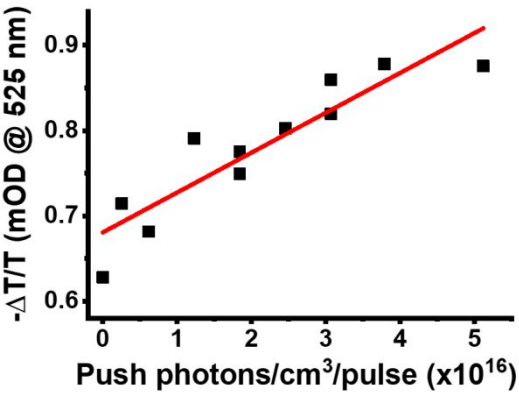

Figure S7. Power dependence of push pulse on ΔOD transient absorption signal at 525 nm. A linear dependence with signal intensity and push power implies the change in the signal due to the push pulse is a single-photon process.

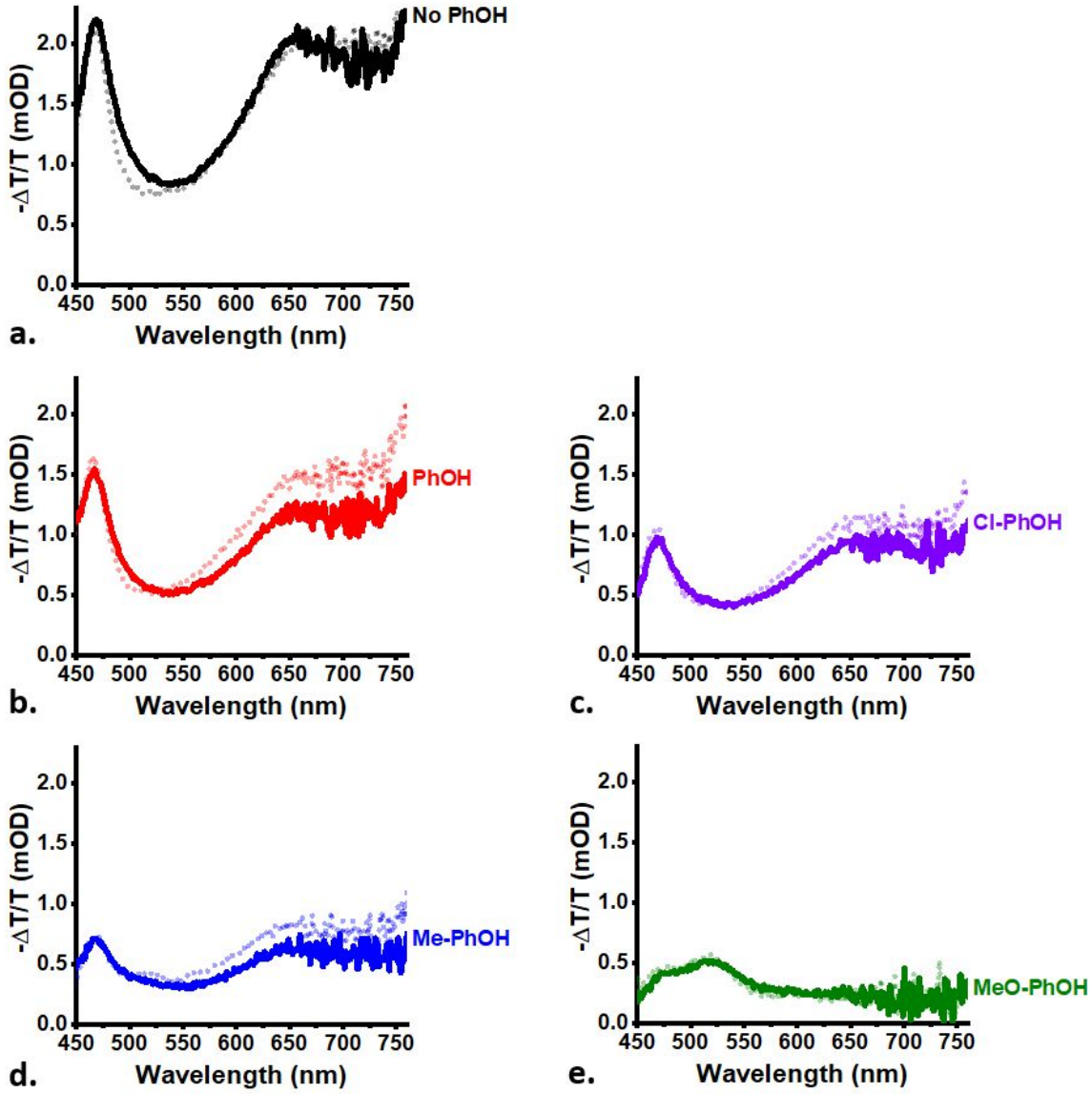

Figure S8. Pump-push-probe spectra of TAHz (50 μM) in the presence of R-PhOH (1.0 M) with and without the push pulse (solid lines and dotted lines, respectively) averaged from 6.5 – 8.0 ps. The decrease in spectral intensity with the push pulse implies a loss of the excited-state hydrogen bonded species. MeO-PhOH (e) has very little change in spectra intensity with the push pulse, implying the push pulse did not considerably change the excited-state population. The system was pumped at 365 nm and pushed at 1150 nm at roughly 6 ps.

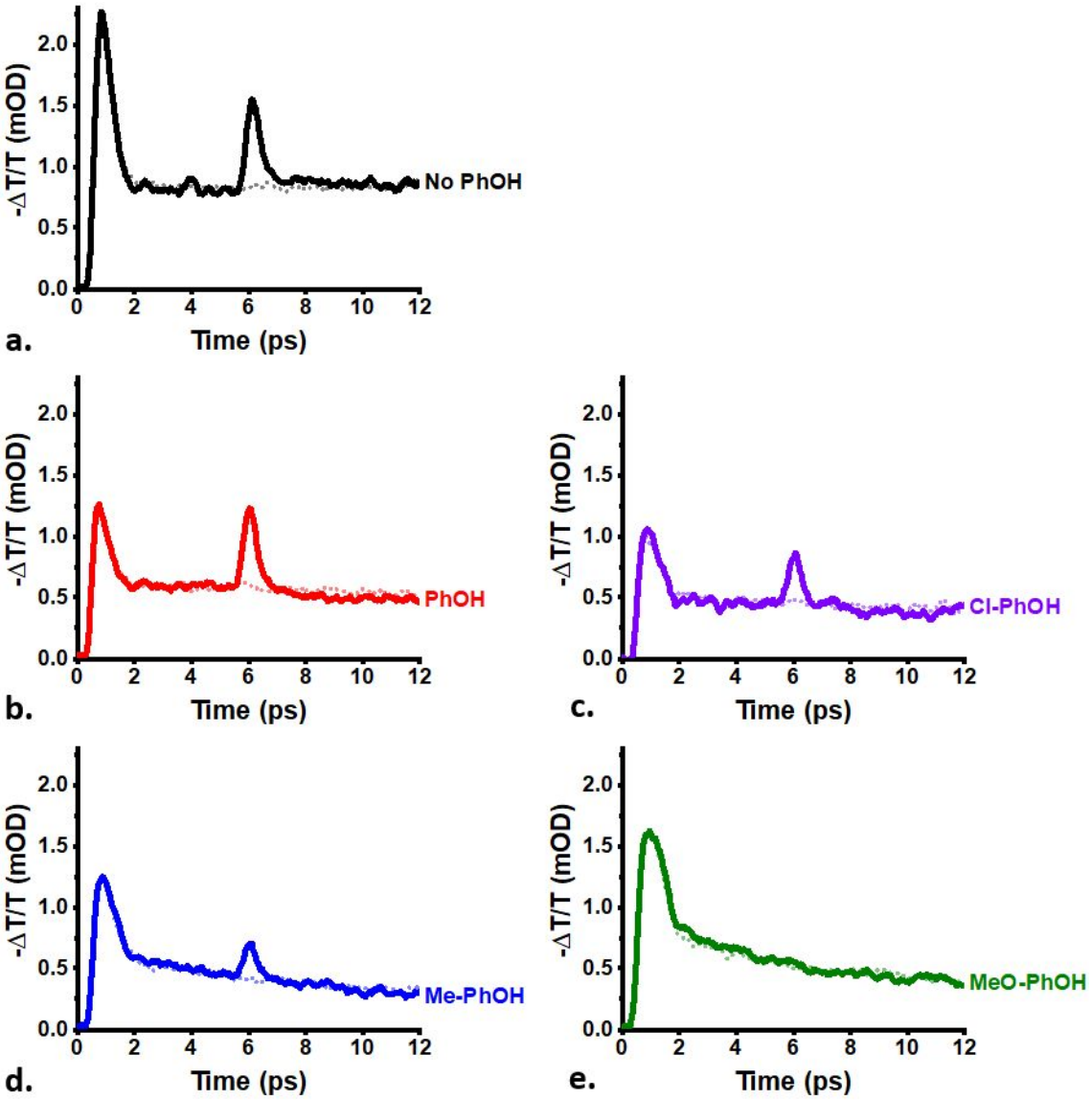

Figure S9. The decay of the excited-state population of TAHz (50 μM) in toluene monitored from 500-550 nm in the presence of R-PhOH (1.0 M) with and without the push pulse (solid lines and dotted lines, respectively). The short-lived species could be the absorption of a higher lying state that quickly relaxes. In the presence of MeO-PhOH (e), the push pulse does not readily populate this higher lying excited state. The system was pumped at 365 nm and pushed at 1150 nm at roughly 6 ps.

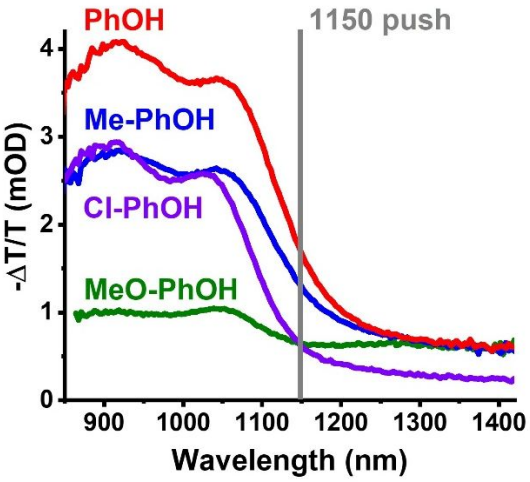

Figure S10. Pump-probe spectra of TAHz (50 μM) in the presence of R-PhOH (1.0 M) averaged from 6.5 – 8.0 ps with reference to the energy of the push pulse used in this work.

SECTION III: COMPUTATIONAL RESULTS

Table S1. Vertical excitation energies (ΔE/eV) and oscillator strengths (*f*) from the ground state (S0), dipole moments (μ/Debye), and dominant electronic configurations of TAHz:R-PhOH complexes, computed with the ADC(2)/cc-pVDZ method at the MP2/cc-pVDZ ground state equilibrium geometry. The *inter*-molecular $\pi\pi^*$ CT state (from R-PhOH to TAHz) is marked in blue. The *intra*-molecular $\pi\pi^*$ CT states (from anisole, A, to Hz) are marked in red. The relevant frontier molecular orbitals are shown in Fig. S11.

State	R												Dominant orbital transition
	Cl			H			Me			MeO			
	ΔE	*f*	μ	ΔE	*f*	μ	ΔE	*f*	μ	ΔE	*f*	μ	
$^1\pi\pi^*$ (LE Hz)	2.65	0.0037	5.19	2.65	0.0028	3.27	2.64	0.0026	2.99	2.64	0.0027	2.12	HOMO-5 → LUMO (69.6%)
$^1\pi\pi^*$ (A → Hz)	3.45	1.1116	4.83	3.45	1.170	5.00	3.46	1.0492	5.82	3.46	1.1125	6.26	HOMO-1 → LUMO (77.0%)
$^1\pi\pi^*$ (A → Hz)	3.60	0.8018	3.01	3.62	0.7926	1.43	3.62	0.7908	1.46	3.62	0.7918	2.58	HOMO-2 → LUMO (77.0%)
$^1\pi\pi^*$ (CT)	3.64	0.0000	10.11	3.63	0.0001	13.92	3.43	0.0649	20.54	3.09	0.0010	24.27	HOMO → LUMO (62.9%)
$^1\pi\pi^*$ (A → Hz)	4.11	0.5666	11.51	4.12	0.5783	8.87	4.12	0.5803	7.83	4.13	0.5521	7.31	HOMO-4 → LUMO (48.7%)

Table S2. Vertical excitation energies (ΔE*/eV) and oscillator strengths (*f) from the first singlet excited state (S_1), dipole moments (μ/Debye), and dominant electronic configurations of TAHz:R-PhOH complexes, computed with the ADC(2)/cc-pVDZ method at the ADC(2)/cc-pVDZ equilibrium geometry of the first singlet excited state. The *inter*-molecular $\pi\pi^*$ CT state (from R-PhOH to TAHz) is marked in blue. The *intra*-molecular $\pi\pi^*$ CT states (from anisole, A, to Hz) are marked in red. The relevant frontier molecular orbitals are shown in Fig. S11.**

State	R												Dominant orbital transition
	Cl			H			Me			MeO			
	ΔE*	*f**	μ	ΔE*	*f**	μ	ΔE*	*f**	μ	ΔE*	*f**	μ	
$^1n\pi^*$ (n → Hz)	1.08	0.0029	4.41	1.08	0.0010	3.28	1.12	0.0014	2.63	1.09	0.0039	1.93	HOMO-1 → LUMO (52.2%)
$^1\pi\pi^*$ (A → Hz)	1.09	0.0043	3.34	1.10	0.0069	4.74	1.09	0.0052	1.56	1.11	0.0028	3.09	HOMO-1 → LUMO (63.3%)
$^1\pi\pi^*$ (A → Hz)	1.25	0.0153	4.58	1.26	0.0130	2.18	1.26	0.0123	1.89	1.26	0.0124	2.38	HOMO-2 → LUMO (69.7%)
$^1\pi\pi^*$ (CT)	1.27	0.0065	15.58	1.26	0.0064	11.86	1.00	0.0070	19.06	0.67	0.0089	24.57	HOMO → LUMO (55.0%)
$^1\pi\pi^*$ (A → Hz)	1.81	0.0104	12.17	1.83	0.0184	10.09	1.83	0.0213	9.67	1.82	0.0368	6.54	HOMO-4 → LUMO (68.4%)

93a' LUMO	61a" HOMO	60a" HOMO-1
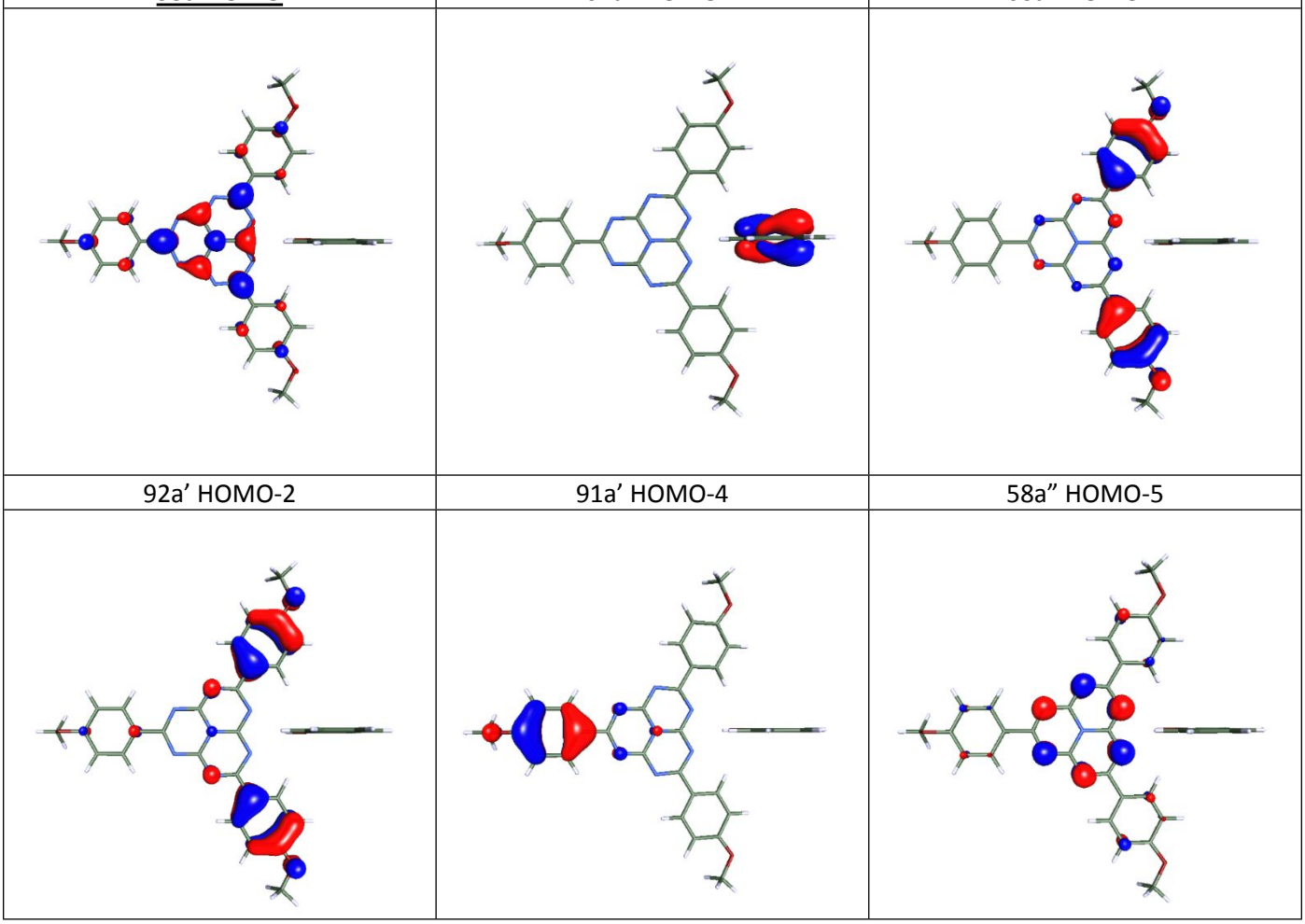		
92a' HOMO-2	91a' HOMO-4	58a" HOMO-5

Figure S11. Hartree-Fock molecular orbitals involved in the excitation of the lowest excited electronic singlet states of the TAHz:PhOH complex. The S_0 state has the configuration $(6a'')^2(61a'')^2$. Note that the C_s symmetry plane is perpendicular to the plane of TAHz.

REFERENCES

1. Rabe, E. J.; Corp, K. L.; Sobolewski, A. L.; Domcke, W.; Schlenker, C. W., Proton-Coupled Electron Transfer from Water to a Model Heptazine-Based Molecular Photocatalyst. *J. Phys. Chem. Lett.* **2018,** *9* (21), 6257-6261.

2. Snellenburg, J. J.; Laptenok, S. P.; Seger, R.; Mullen, K. M.; Stokkum, I. H. M. v., Glotaran: AJava-Based Graphical User Interface for theRPackageTIMP. *J. Stat. Softw.* **2012,** *49* (3), 22.

3. Pinteala, M.; Schlick, S., Direct ESR Detection and Spin Trapping of Radicals Generated by Reaction of Oxygen Radicals with Sulfonated Poly(Ether Ether Ketone) (SPEEK) Membranes. *Polym. Degrad. Stab.* **2009,** *94* (10), 1779-1787.